Progress in Nuclear Energy 160 (2023) 104689

Contents lists available at ScienceDirect

Progress in Nuclear Energy

journal homepage: www.elsevier.com/locate/pnucene

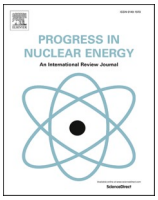

Analysing the performance of radiological monitoring network during nuclear accidents

M. Sangiorgi [a,*], M.A. Hernández-Ceballos [b], J.P. Bolivar [c]

[a] Joint Research Center, Ispra, Italy
[b] Department of Physics, University of Córdoba, Spain
[c] Department of Applied Physics, University of Huelva, Spain

ARTICLE INFO

Keywords:
JRODOS
EURDEP
Nuclear
Emergency preparedness and response
EP&R
Seasonal meteorology

ABSTRACT

JRODOS was used to simulate the dispersion of airborne radioactive material from a point source over the period 2012–2015. In total, 1331 radioactive plumes were simulated with the objective to investigate the influence of changes in meteorological conditions in the performance of the monitoring network. For this purpose, the existing set of 84 monitoring stations included in the EUropean Radiological Data Exchange Platform (EURDEP) system in an area of 200 km around the source point is taken as reference. A methodology is presented for quantitative evaluation of the variability of the number of stations affected, the time of the first detection, the maximum registered and differences between the maximum values match in the network and in the simulated plumes. The results show seasonal differences in all of these parameters according to changes in the size and shape of the affected area due to meteorological conditions. There are large differences in the number of monitoring stations affected by the plumes, from 2 to 74; in the timing and location of the first alert given by the network, from 1 to more than 5 h and faster along the west-east axis from the source; and in level of maximum gamma dose rate detected by the monitoring stations, from 0.17 nSv/h in summer to 0.22 nSv/h in autumn. These results show the need to consider this type of analysis over the years in the design of monitoring networks and in the development of nuclear emergency preparedness and response (EP&R) plans.

1. Introduction

Emergency Preparedness and Response (EP&R) plans provide information and tools on how to prepare and train for emergencies and for the associated hazards (Casajus Valles et al., 2021). Within the wide variety of possible emergencies and related EP&R plans, i.e. from natural events (earthquakes, floods, fires …) to man-made events (terrorism, radiological dispersal devices (RDDs)), nuclear EP&R aims to minimise the impacts of nuclear and radiological disasters regardless of whether they result from accidents, negligence or deliberate acts (IAEA, 2015). In general, the aim of this strategy is to facilitate decision-making by providing available/needed information in both the preparedness and the emergency phases (Handl, 2020; Song et al., 2021).

In general, the first step in developing an EP&R plan is to conduct a risk assessment to identify potential emergency scenarios (Ashley et al., 2017). Detecting anomaly conditions in nuclear reactor is a critical issue in safety management of Nuclear Power Plants (NPPs) (Yong and Linzi 2022). In this sense, nuclear EP&R plans must address scenarios ranging from minor accident (e.g. a small spill of radioactive material) to a major nuclear accident with a large-scale release of radioactivity (such as Chernobyl or Fukushima). In particular, in the case of an event with an off-site impact, nuclear EP&R seeks to prevent or at least reduce as far as possible the negative effects of ionising radiation on the population and the environment. In order to achieve this main objective, and in the early phase of an event with a release to the atmosphere, emergency monitoring data are the basis for gaining knowledge about the dynamics of the accident and, consequently, accuracy data, in time and space, are a necessary and relevant input to support decisions on the implementation of countermeasures and to validate and update predictions (OECD/NEA, 2000).

These measurements, such as the ambient equivalent dose or the ambient equivalent dose rate, can be made using different types of detectors, e.g. fixed stations, monitoring teams with portable instruments and aerial measurements. Many countries have monitoring networks consisting of several real-time radioactivity monitoring stations, whose measurements are collected and continuously supervised by emergency

* Corresponding author.
E-mail address: Marco.SANGIORGI@ec.europa.eu (M. Sangiorgi).

https://doi.org/10.1016/j.pnucene.2023.104689
Received 23 January 2023; Received in revised form 9 March 2023; Accepted 5 April 2023
Available online 15 April 2023

centers (Abida et al., 2008) (Yang, 2014) (Ontalba et al., 2022). The arrangement and spatial density of networks dealing with atmospheric nuclear and radiological releases varies from country to country according to the needs and criteria defined by national authorities. An example of this variability is easily seen by visiting the European Radiological Data Exchange Platform (EURDEP), which is the near-real-time exchange system for unvalidated radiological monitoring data from most European countries (Sangiorgi et al., 2020). These networks must be able to detect gradual changes, background patterns and extreme values affecting the population and/or environment during an emergency. Therefore, network design is a key factor in ensuring the usefulness and representativeness of the measured data. In particular, in the initial phase of the radioactive release, they must be able to quickly detect the release, as well as the associated maximum values, e.g. (Melles et al., 2011); (Urso et al., 2012).

The response of a monitoring network to the accidental leaks is jointly determined by the release rate and the meteorology. The temporal variation of the release rate may change the TGDR (Li et al., 2019), as well as several authors (e.g. (Povinec et al., 2013), (Masson et al., 2018), (Guttikunda and Gurjar, 2012), (Jayamurugan et al., 2013), (Gogikar and Tyagi, 2016), (Gogikar et al., 2018), Kristiansen et al., 2016; Sato et al., 2020; Zhuang et al., 2023) have demonstrated the influence of meteorological conditions on the shape of a plume carrying contaminants and on the atmospheric lifetime of radionuclides emitted from a point source on a local and regional scale. In essence, radioactive plumes can spread far and wide depending on the temporal and spatial variation of meteorological parameters, such as rainfall or wind direction and speed, which, in addition, vary throughout the year. Considering this temporal variability, i.e., annual variations that reflect year-to-year differences or seasonal differences that show intra-annual variations, calculations of all possible dispersion scenarios must be considered for the determination and understanding of activity concentrations and its temporal variability at receiving points. Therefore, this variation in meteorological conditions and its influence on the dispersion of radioactive materials must be included in the evaluation of the monitoring network.

The overall objective of this study is to assess the ability of a monitoring network to detect radiation levels, with a focus on fist alert and maximum values. To achieve this objective, the approach used is based on the influence of meteorological conditions on the dispersion of radioactive material in the atmosphere. This assessment is carried out by simulating 1331 release meteorological scenarios of radioactivity from a chosen point source over the period 2012–2015, i.e. the dispersion of a single source term under different meteorological conditions to evaluate the capability of the monitoring network in detecting the radioactive plume and capturing its spatial and temporal characteristics. These simulations were performed with the RIMPUFF model (Thykier-Nielsen et al., 1999), which is integrated in the JRODOS (Real-time Online DecisiOn Support) decision support system for off-site nuclear emergency management (KIT, 2017). This system is operated nationally but also locally by more than 20 institutions in 16 countries, and it has been used in many scientific researches, following the Fukushima Daiichi accident (e.g. Landman et al., 2014), the ^{106}Ru unusual release (Kovalets et al., 2020) or for simulating routine discharges (Selivanova et al., 2023).

In general, the following research topics are aimed at:

- Analysing the spatial variability of the area affected by plumes under different meteorological scenarios.
- Assessing the ability of the monitoring network to detect plumes under varying meteorological conditions.
- Investigating the influence of seasonal variability of meteorological conditions on the detection times and maximum values recorded in the monitoring network.

The paper is structured as follows: Section 2 introduces the data used in the analysis and the proposed methodology, Section 3 presents the set of results obtained, while Section 4 discusses the usefulness of our results and the importance of meteorological analysis in the EP&R setting. Finally, Section 5 presents the conclusions.

2. Materials and methods

2.1. Study area

The study area focuses on the Almaraz Nuclear Power Plant (hereafter ANPP) (Fig. 1), the largest operational nuclear power plant in Spain, which is located in the Extremadura region near the border with Portugal. This facility is close to several environmental points of interest, including the Sites of Community Importance and the Special Protection Zone of the Monfragüe National Park, the Dehesas del Entorno and of Arrocampo, which are Special Areas of Conservation. The region's climate is continental, with scarce and irregular rainfall.

Fig. 1 shows the location of the release point and the spatial distribution of the 84 monitoring stations considered in this study. All these monitoring stations are included in EURDEP (EUropean Radiological Data Exchange Platform), which is the reference platform in Europe and neighbouring countries for the exchange of radiological monitoring data from automatic monitoring networks in near real time. The data exchanged mainly concern the gamma dose rate and, under normal conditions, provide information on the natural radiation background. For more information about EURDEP we refer to https://remon.jrc.ec.europa.eu/About/Rad-Data-Exchange.

2.2. Source term estimation

The source term depends on the type of the nuclear facility and may be different for each postulated incident or accident (Rudas et al., 2021), so the source term must be determined according to the specific characteristics of the facility. ANPP comprises two pressurised water reactor (PWR) units, which went into operation in September 1983 and July 1984, respectively. The accident chosen in the present analysis is a large break loss of coolant accident (LBLOCA), in which the main coolant circuit is compromised or broken and pumps cannot circulate enough coolant through the core. The associated source term was estimated with the integral code MAAP4 (Modular Accident Analysis Program) (EPRI, 2012) (EPRI, 2012), developed specifically for severe accidents. The source term estimation was performed as part of a project led by the European Commission's Joint Research Centre (JRC), aimed at diagnosing and predicting the progression and consequences of severe accidents in NPPs located in European countries. The source term estimated with MAAP4 is adapted using a methodology developed at the JRC to estimate the dispersion of radionuclides in the environment with other computer codes (Vela-García and Simola, 2016).

The source term lasts 48 h (2 days), with a time step of 1 h (Fig. 2). The total amount of radioactivity released is 2.3 10^{12} Bq, with an initial peak in the first hour and a second between 28 and 33 h. There are three radioactive elements released (^{131}I, ^{137}Cs, and ^{90}Sr), which have been selected due to the greatest health concern for the population during a nuclear accident, i.e. these three isotopes can easily attach to human tissues if ingested and cause internal exposure that will result in a high dose.

2.3. Atmospheric dispersion simulation

To simulate the atmospheric dispersion of the chosen source term, we used the RIMPUFF dispersion model (Thykier-Nielsen et al., 1999), which is included in the JRODOS system. RIMPUF is a Lagrangian mesoscale atmospheric dispersion puff model designed to calculate the concentration and doses resulting from the dispersion of airborne materials. More detailed information on the RIMPUFF model and its use of parameterised puff diffusion, i.e. diffusion coefficient, dry and wet deposition and other considerations, is available in (Mikkelsen et al.,

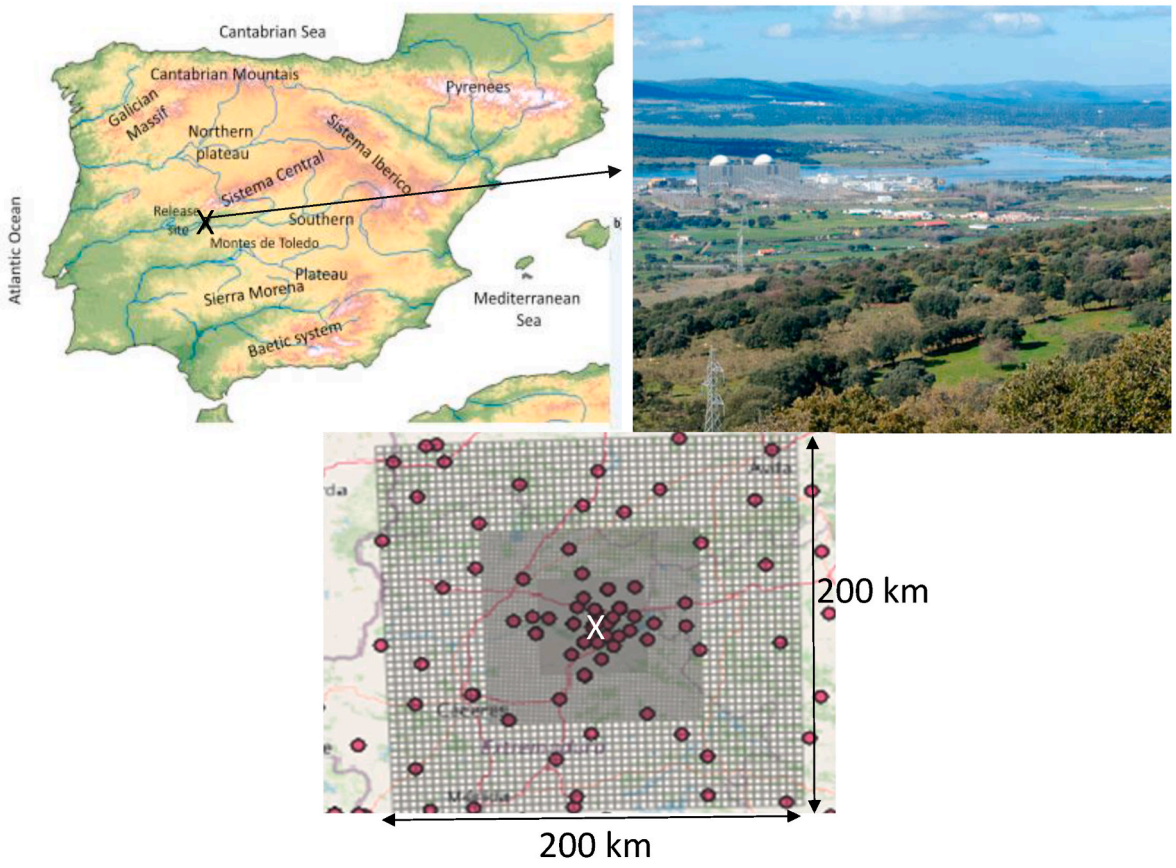

Fig. 1. Study area and the locations of the EURDEP stations in the domain of simulation.

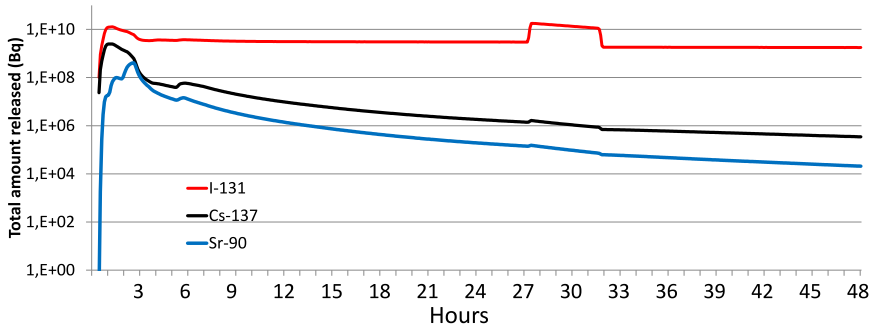

Fig. 2. Temporal evolution of the source term simulated by MAAP and used in the present study.

1984) and (Mikkelsen and Thykier-Nielsen). This model has been used in several analysis (e.g. (Leung et al., 2018), (Hernández-Ceballos et al., 2021).

The computational spatial domain is a 200 km square centred on ANPP (Fig. 1), with a decreasing resolution with distance from the release point: a maximum resolution of 4 km^2 around the release point and 16 km^2 from 50 km to 100 km. This grid spacing was established as a compromise between the need to obtain results in the early phase of the release and the ability of RIMPUFF to be applied to homogeneous and inhomogeneous terrain with moderate topography on a horizontal scale of approximately 100 km. The meteorological data used to simulate the different meteorological conditions (temperature, relative humidity, rain, fog …) and transport process from 2012 to 2015 are produced by the National Centers for Environmental Prediction (NCEP) in the freely available GFS format (Global Forecast System). The temporal resolution of these meteorological data is 6 h and the horizontal spatial resolution is 0.5 × 0.5° (~55 × 55 km^2), covering the pressure range from 1000 to 10 hPa with 26 standard pressure levels.

The JRODOS meteorological preprocessor (Andronopoulos et al., 2010) takes that input data to perform spatial interpolation and compute the meteorological information on the selected grid and performs a "wind field model" to adjust the interpolated wind speed components to ensure conservation of the wind field mass.

Daily dispersion simulations from 2012 to 2015 were performed automatically using the statistical tool implemented in JRODOS. During this period, 1331 dispersions of a continuous 48-h time span were simulated. This means approximately 91% of the possible simulations in this period, thus ensuring a large statistical sample for the present analysis. Fig. 3 shows the monthly and daily distribution of these 1331 simulations. The monthly number of simulations varies from 106 (September) to 120 (January, July, November, December). These numbers make it possible to have a sufficient number of simulations for

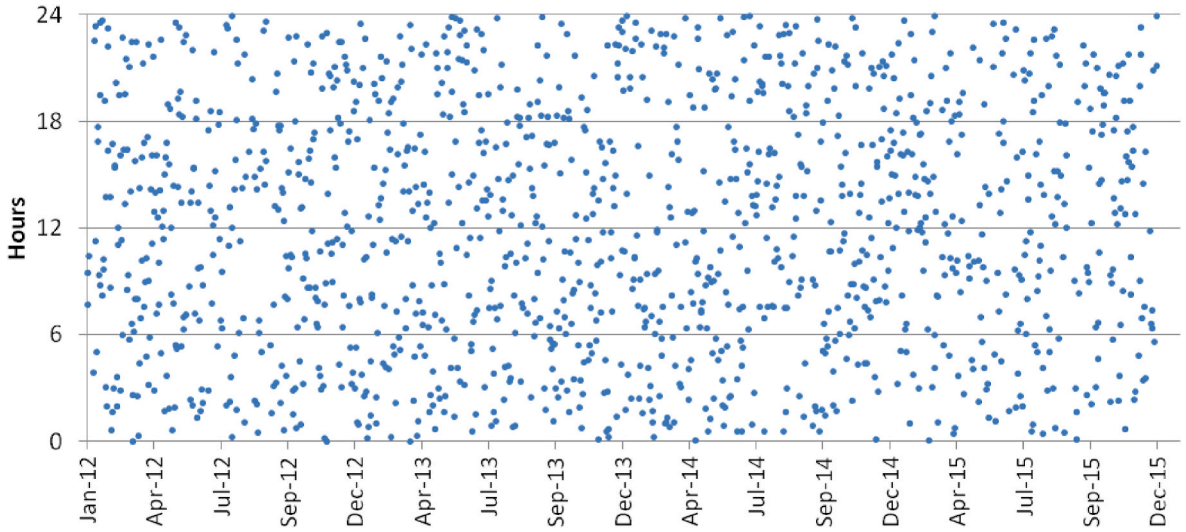

Fig. 3. Start of the simulated radioactive releases over the analysed 4-year period.

each month/season, thus covering the entire framework of weather scenarios over the studied region. In this analysis, each seasons is defined as winter (December to February, 343 simulations), spring (March to May, 337 simulations), summer (June to August, 323 simulations), and autumn (September to November, 328 simulations). Furthermore, the fact that radioactive releases were simulated using different start times (Fig. 3), ensures that different atmospheric stability conditions are covered in the early hours of each daily release.

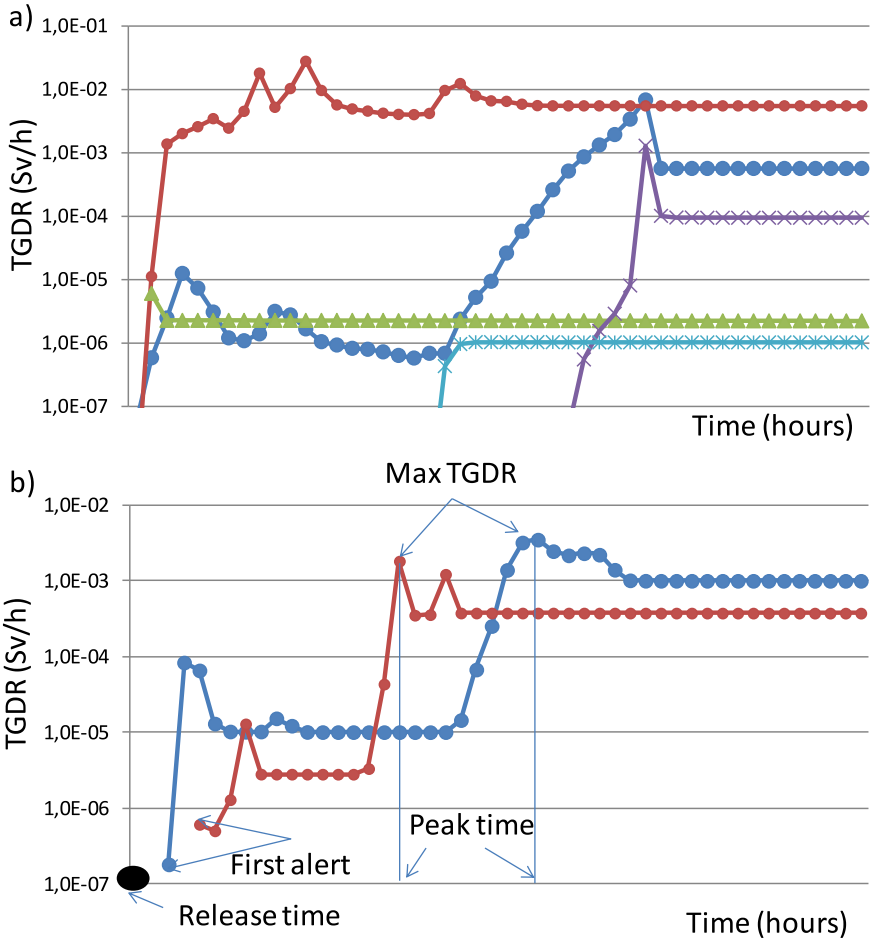

Fig. 4. a) Example of five modelled TGDR time series representing the passage of the plume over five different stations during a release, and b) identification of some of the parameters used in the current study. The black dot on the X-axis indicates the plume release time.

2.4. Parameters for evaluating EURDEP network

Following the methodology applied in (Hernández-Ceballos et al., 2020), hourly time series of Total Gamma Dose Rate (hereafter TGDR) were extracted for each simulation at each monitoring station (Fig. 4a). For the present analysis, a threshold rate of 100 nSv/h is applied, and hence, those values below this threshold are discarded. This high threshold is compatible with the need to subtract the natural background, and to limit the occurrence of false radiological alarms associated, for instance, to radon peaks (Cinelli et al., 2014). To analyse and quantify the performance of the monitoring network in detecting plumes in both time and space under different weather scenarios, we focused on the time and place of first alert and the maximum TGDR values in the network and plume. For this purpose, we extracted the following parameters for each simulation and monitoring station:

- First alert in time [hours]: Time elapsed from the start of the release to the first TGDR value above 100 nSv/h recorded.
- Maximum activity [nSv/h]: Maximum TGDR recorded at each monitoring station.
- Peak time [hours]: Time elapsed from the release to the maximum TGDR value recorded at each monitoring station.
- Maximum activity in plume [nSv/h]": Maximum TGDR simulated in plume in each daily release.

Fig. 4b shows two examples of modelled TGDR values (in logarithmic scale) representing the passage of the plume at five different stations during two different releases to illustrate some of the parameters used in the current study.

3. Results and discussions

3.1. Affected areas

Once released into the atmosphere, as the plume travels downwind, the diameter of the plume usually grows and gradually spreads and disperses; therefore, the first objective of this analysis is to identify those areas that could be most affected by these potential emissions. Fig. 5 shows the seasonal spatial variability. This plot represents those grid cells with a frequency of more than 10% of registering TGDR greater than 100 nSv/h in the period 2012–2015, i.e., at least 6389 h out of (1331 simulations x 48 h = 63888 h).

This figure shows a main dispersion along the west-east axis from the source, which is clearly related to topographical effects and regional atmospheric dynamics. The ANPP is located at the far end of the Arrocampo basin in the Tajo river valley, which widens to the east and narrows to the west, flanked by mountains up to 1000 m above sea level to the north and south. This configuration, together with the high influence of western flows (Hernández-Ceballos et al., 2020), favours the channelling and eastward movement of the dispersed plume through the valley. Within this general behaviour, there is great variability in the areas most affected, in terms of shape and size, depending on the season. These figures clearly show a larger affected area in summer and a smaller one in autumn, winter and spring. This seasonal difference is associated with changes in weather patterns, such as the development of mesoscale processes in summer, limiting long-distance transport from the source point, and more synoptic situations in other seasons causing larger wind speeds, and hence, dispersion processes (e.g. Jin et al., 2021; Ma et al., 2022). The main affected areas are to the east of the release point, while in autumn and spring there is a western area, similar in size to the eastern area in autumn. This distribution agrees with the frequency of air mass patterns identify in Hernández-Ceballos et al. (2020). These results highlight the combined effect of local and regional geographical characteristics and variation of wind flow pattern in the atmospheric dispersion of a hypothetical radioactive plume and, consequently, their influence in the most affected areas.

3.2. Detection of plumes by the monitoring network

All 1331 simulated plumes are detected by this monitoring network (Fig. 1), but each plume differently. There is a large variation in the number of stations recording the passage of a single plume within 48 h, i.

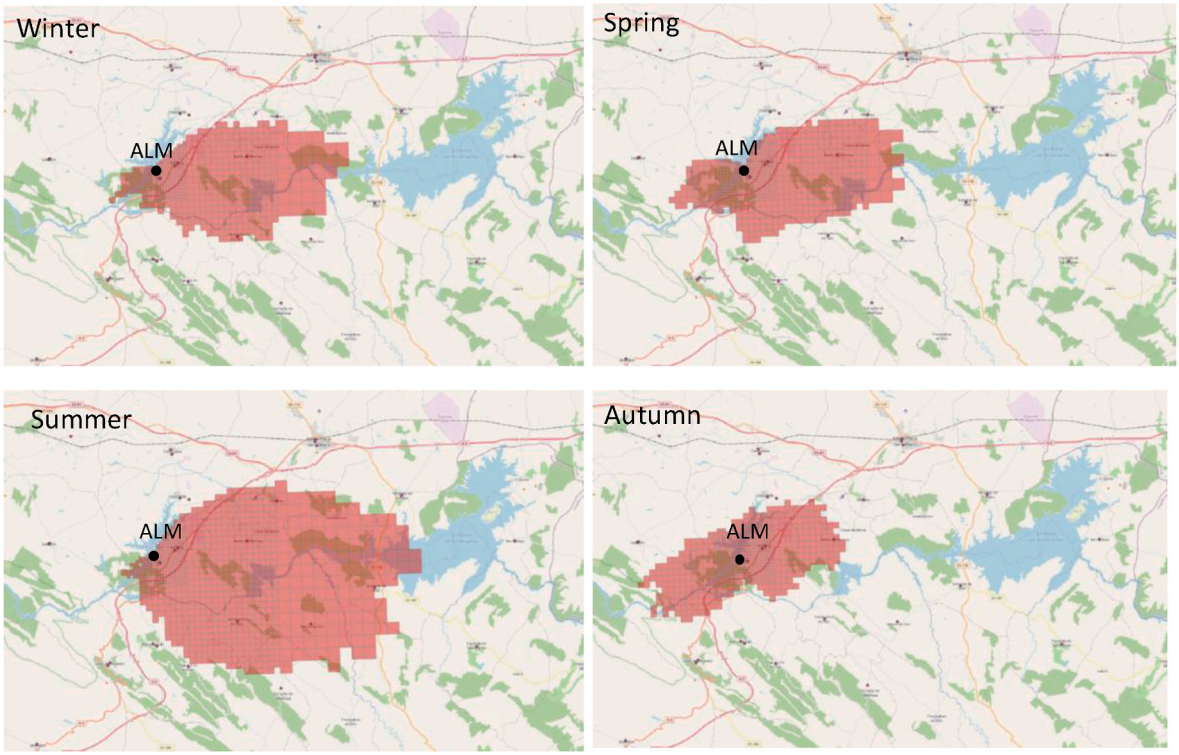

Fig. 5. Seasonal geographical distribution of grid cells with a frequency of more than 10% recording TGDR values above 100 nSv/h in the period 2012–2015.

e., the minimum number is 2 stations occurring in 2 plumes, while the maximum is 76 out of 84 monitoring stations, occurring in 4 plumes. Fig. 6 shows the number of plumes detected by a certain number of stations within 48 h, and the cumulative frequency graph. During the entire study period, the maximum number of plumes detected by the same number of stations is reached between 17 and 27 stations, with the number of plumes detected decreasing as the number of stations increases. These results indicate that there is a large percentage of stations that are not impacted by plumes. On average, 35% of stations (30 out of 84) would be impacted by plumes, while the others would be mostly ignored in most meteorological scenarios.

Fig. 6 also shows the large seasonal variability in the number of stations affected by plumes. It can be seen that in winter, spring, and autumn there are many plumes that are detected by only a few stations, while in summer plumes affect a larger number of stations within 48 h. These results are in line with the spatial coverage and differences in shape and size of the most affected areas (Fig. 4), and are partly justified by seasonal changes in synoptic situations that imply the development of mesoscale circulations, and thus different dispersion patterns. In this sense, studies on atmospheric circulations over the Iberian Peninsula (e.g. (Hoinka and De Castro, 2003); (Palau et al., 2005)) have shown particularities related to spring, summer, and early autumn dynamics with the development of mesoscale processes associated with the thermal low pressure region in the centre of the Peninsula. This meteorological scenario favours recirculation and stagnation processes, and can therefore increase, in this specific case, the travel time of the radioactive plume in the same area near the ANPP, and thus the number of stations affected. In contrast, winter weather scenarios are more associated with the influence of westerly synoptic flows, which increase the distance travelled by the plume and thus reduce the dwell time in the area close to the ANPP, and thus the number of stations affected.

Fig. 6 also shows the number of stations required to reach a steady state in the monitoring network for plume recording, i.e. the saturation point, which is described as the point in the data analysis at which new incoming data yields little or no new information useful for achieving the objectives of the study (Guest et al., 2020). In the present study, this saturation point is considered as the number of stations from which the number of detected plumes stabilizes on the monitoring network. To identify this, an information threshold of $\leq$5% was selected; in this case, the saturation number of the current monitoring network for the entire period is 29, i.e. 53 % of the detected plumes. This different distribution means that the number of stations required to reach saturation varies from 27 in autumn and winter to 32 in summer, which is in agreement with the total average number of stations detecting plumes in summer (34) and winter (28).

To investigate whether the distance from the source correlates with plume detection, Fig. 7 shows the scatter plot between the frequency of plumes detected by each monitoring station and the downwind distance from the source of each of them. This analysis shows that there are six stations that detect more than 60% of the simulated plumes, while, on the contrary, there are 36 stations that only manage to detect 30% of the simulated plumes. Considering the distance from the source, Fig. 7 shows a clear decrease in the number of plumes detected by each monitoring station with distance. The three closest stations detect more than 70% of the plumes; the station located on the premises of the ANPP is the only one with a rate of 100%, while stations located between 10

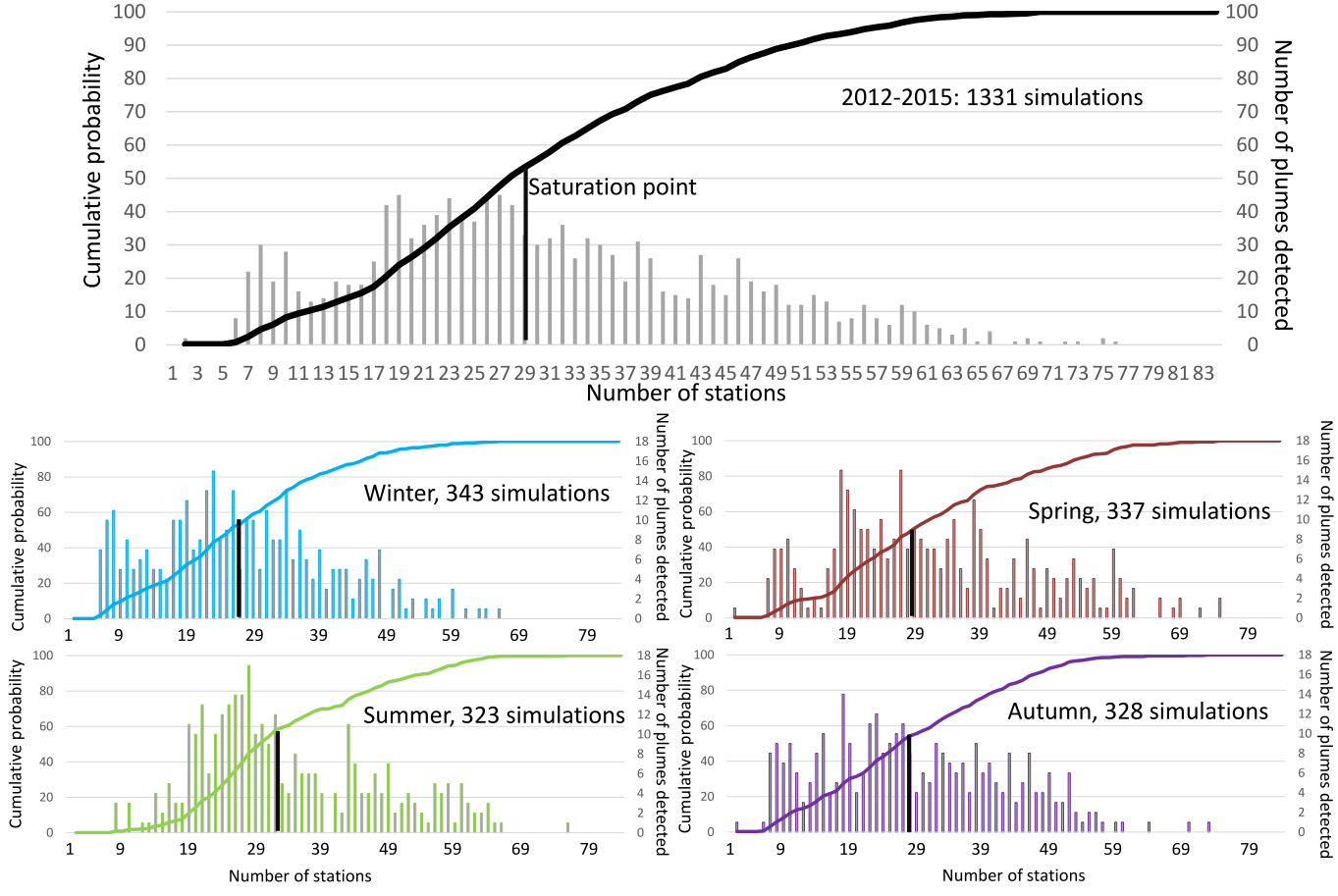

Fig. 6. Variation of the number of plumes detected with the number of monitoring stations, and cumulative probability graph of the monitoring network for the set of simulations and grouped by season.

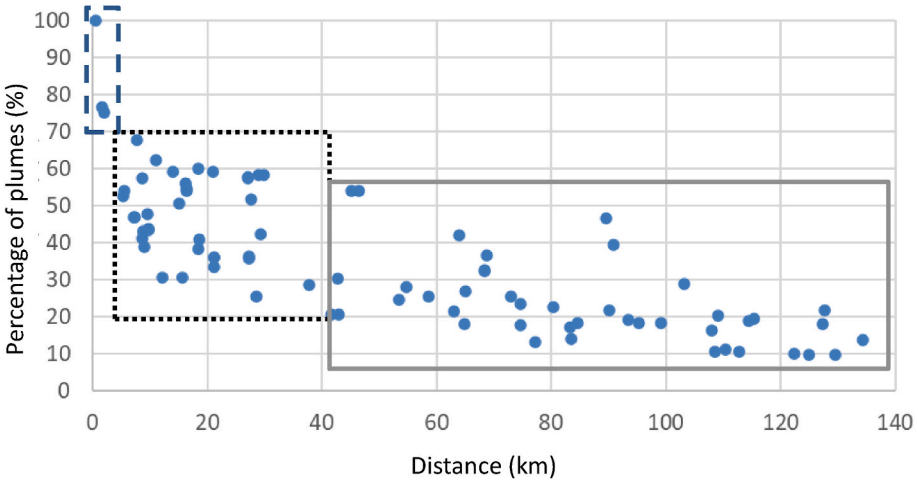

Fig. 7. Scatter plot of the percentage of plumes detected by each sensor and the distance from the source of each sensor. Each point represents one EURDEP station in Fig. 1.

and 40 km show great variability in the percentage of plumes detected (70-25%). In this sense, the detection rate between 10 and 40 km is almost independent of distance. This fact may be associated with the influence of changing meteorological scenarios, as well as the short distance travelled by the plume from the source, which limits the dilution of radioactivity concentrations. From 40 km onwards, the detection rate of the plume decreases at most stations, with a minimum detection of 10% of the plumes at the farthest distances (over 100 km from the source).

Finally, as meteorological factors vary mainly over time and follow seasonal patterns, we analyse seasonal changes in the number and spatial distribution of the stations concerned. On average, the number of stations detecting plumes varies from 27 in winter to 34 in summer, while it is 32 in spring and 29 in autumn. Fig. 8 shows the spatial distribution of the stations around the source and groups the stations according to the season in which the maximum number of plumes is detected. Whereas in spring, stations located to the south of the source are mainly affected, in autumn these stations are located to the northwest. Fig. 8 also shows that stations located east of the source are affected in summer, while those close to the source are more exposed in winter.

3.3. First alert

The ability of a monitoring network to quickly detect a release, i.e. the first alert, is a key factor in deciding and implementing protective countermeasures. Moreover, especially in the early stages following a release, detailed quantitative monitoring data are very useful for validating and/or refining model predictions on which certain countermeasures have been or will be based. Therefore, the faster the network detects the plume, the earlier this information is available.

Analysis of the first warning parameter indicates that 76% of the 1331 plumes are detected within the first hour after release, while 13% are detected within 2 h and only 1.8% are detected between three and 7 h after release. According to the seasons, while in summer 86% of the plumes are detected within the first hour, this number decreases to 64% in autumn, while it is similar in winter and spring (76%). These results show that the source point is well covered by this monitoring network, albeit with clear seasonal differences in the first hour after release. However, in each season, over 84% of the plumes are detected within 2 h. On average, and for the entire monitoring network, the first alert interval ranges from 10 to 3 h in winter, 9 to 3 h in spring, 13 to 2 h in summer and 8 to 4 h in autumn. These seasonal changes can be explained by the rainfall regime in the region. The influence of precipitation on the decrease in the amount of material released into the atmosphere over time is well known; for example, a precipitation rate of 4 mm/h can lead to the removal of half of the material in the plume from the atmosphere in less than an hour, while a precipitation rate of 0.5 mm/h can reduce the plume by 50 per cent in just 4 h (Leadbetter, 2019). This region is characterised by low and irregular rainfall, with a rainy season in November and dry periods mainly in June, July and August (García-Marín et al., 2012). The lower amount of precipitation in

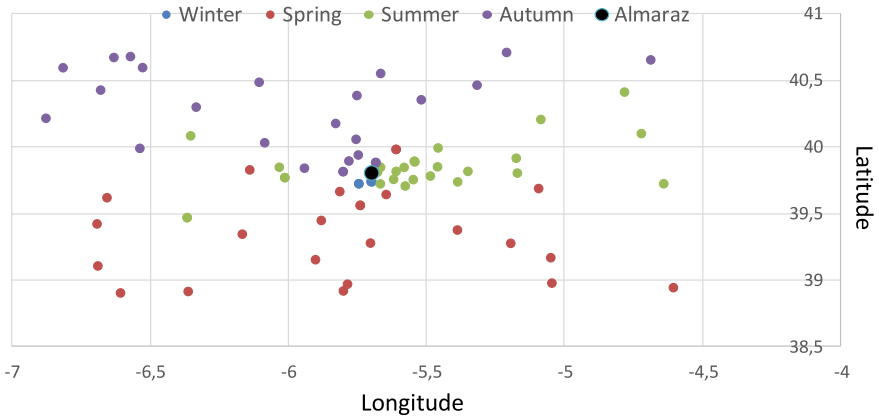

Fig. 8. Spatial distribution of sensor from the source and the season in which each is most affected by plumes. Each point represents one EURDEP station in Fig. 1.

summer can cause the radioactive plume to spread more widely and, consequently, increase the possibility of passing over more monitoring stations than during rainy periods, when the scavenging effect washes particulate matter from the atmosphere and, consequently, limits the dispersion and/or transport of the radioactive plume.

Complementing these results, Fig. 9 presents the time interval in which each station detects the maximum number of plumes for the first time. This figure provides a picture of the speed at which the plume disperses and is detected by the stations, i.e. the smaller the time, the faster the plume. Fig. 9 shows that plumes dispersing along the west-east axis are detected within the first 4 h (green dots), while, in contrast, plumes moving in other directions are initially detected within 8–12 h. In this sense, plumes heading north-west are mostly detected within 8–10 h, while those heading north-east within 10–12 h. This result, in general, indicates difficulties with increasing time and distance from the source, as well as according to the direction taken by the plume with respect to the source.

3.4. Maximum concentrations

As expected, the average maximum TGDR detected at the monitoring stations decreases with distance from the source point (not shown). The correlation coefficient between the two over the entire period is −0.48. On average, the maximum TGDR detected by the monitoring network ranges from 4.77×10^{-6} Sv/h to 3.67×10^{-2} Sv/h, which corresponds to two stations located 0.6 km and 130 km from the source, respectively. Fig. 10a shows the seasonal variability of the maximum TGDR values with distance. It can be seen that large distances from the source show seasonal differences in the maximum values. This distribution agrees with the results shown in Fig. 7 and confirms the great seasonal influence at stations located 40 km and above. In general, the lowest maximum values at these stations occur in summer and the highest in winter. These results are confirmed in Fig. 10b, where the stations are grouped according to the season in which the maximum TGDR is recorded at each of them. This analysis reveals that the highest TGDR values are recorded mainly in winter (60% of monitoring stations), while only 2.3% of monitoring stations record the highest TGDR in summer. These percentages are similar in spring and autumn, with around 18%. It is interesting to note that this 2.3% in summer corresponds to stations close to the source, while stations located to the north are those that record the maximum TGDR in spring. In this sense, the weak convective activity meant that the atmospheric boundary layer was shallower in winter than in summer, thus limiting the transport of substances and increasing the possibility of reaching high TGDR concentrations in winter.

The analysis of how well the monitoring network is able to capture the maximum in the plume and assess its possible seasonal variability is important, for example, to make estimates of the source term. This comparison reveals a general under-detection of the maximum in the plume by the network. The simulated peaks in the plume average about 0.23 nSv/h, while the network peaks are about 0.06 nSv/h. The differences between the maximum concentrations in the plumes and in the network range from 0.17 nSv/h to 1.92 nSv/h. The seasonal analysis shows differences between the seasons from 0.17 nSv/h in summer to 0.22 nSv/h in autumn. To quantify this difference between the maximum concentrations in the plume and in the network, the intensity performance (hereafter PI) is calculated as the ratio between the maximum simulated TGDR in the entire model domain and the maximum simulated TGDR value recorded by any of the stations at any time of the plume passage. On average, the PI increases with distance (Fig. 11), which reinforces the fact that the further the plume moves away from its point of origin, the more difficult it is for the monitoring network to capture the maximum concentration in the plume. On average, the ratio increases from 2.0 to 4.0, as it is difficult to detect the maximum value even at monitoring stations very close to the source point. Finally, knowing that the maximum in the plume is mostly identified close to the source, the distance between the maximum in the plume and in the network is calculated. On average, this distance is about 5 km, although it shows seasonal variability, being about 2 km in summer and 7 km in winter. This seasonal influence is clearly visible when considering the maximum distance between the two values over the entire period, which is about 21 km in summer and about 115 km in autumn, 84 km in winter and 95 km in spring.

4. Implications in EP&R

This methodological approach is based on the generation of massive amounts of atmospheric simulations with the aim of considering as many transport and dispersion scenarios as possible over a certain region, so that statistical analysis leads to the extraction of representative information on dispersion patterns (e.g. (Urso et al., 2012); (Kopka et al., 2022)). On this basis, the results demonstrated a clear influence of meteorological scenarios on the response of the monitoring network in providing the first alert and capturing the maximum TGDR concentrations associated with the dispersion of hypothetical airborne radioactive material from a point source. These differences clearly support the need to assess and characterise the response of the monitoring network to a radioactivity release under a full range of meteorological scenarios, and not just provide a snapshot of a single study period.

The results of this process can help optimise nuclear EP&R plans,

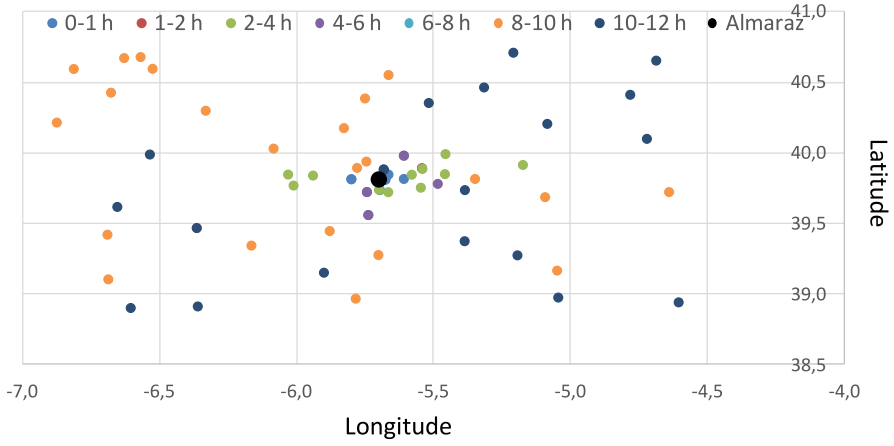

Fig. 9. Distribution of sensors according to the time interval in which the maximum number of plumes are detected for the first time. Each point represents one EURDEP station in Fig. 1.

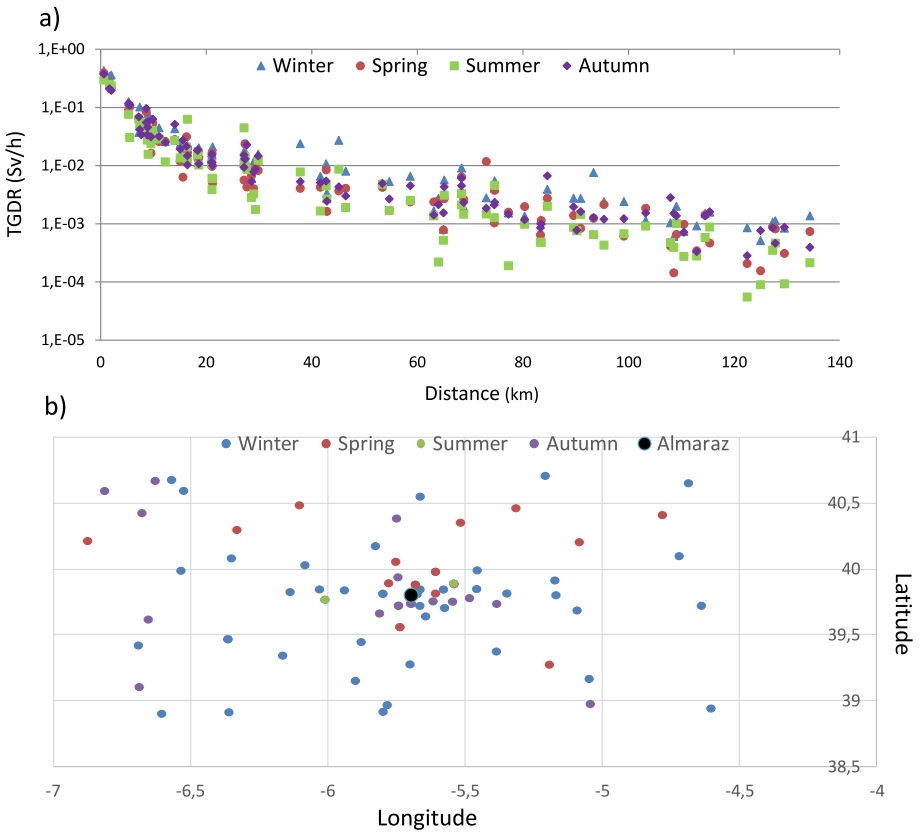

Fig. 10. a) Seasonal variation of maximum TGDR with distance and b) distribution of sensors according to the maximum TGDR values. Each point represents one EURDEP station in Fig. 1 (bottom figure).

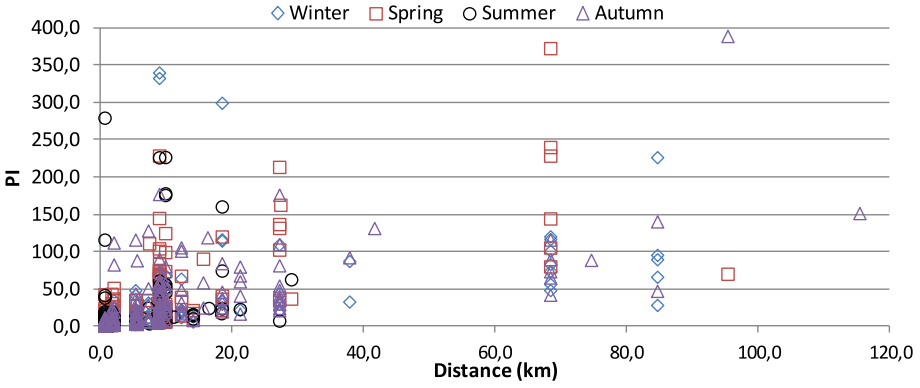

Fig. 11. Scatter plot of seasonal variation of PI with distance from source.

which must take into account the time when measurements are taken, with respect to the time phases of the accident, and the place where measurements are taken, with respect to the defined geographical zones. With this methodological approach, it is possible to produce figures such as Fig. 5, which can be used to adapt the emergency and food restriction zones according to weather scenarios or seasons, and the planning radius for Category I and II facilities, as suggested by (IAEA, 2003). In fact, instead of simply delimiting areas with approximate circles, with this approach it is possible to estimate and delimit highly affected areas, i.e. the seasonal variability of affected areas, indicating which areas are more likely to be exposed depending on the month or season in which the release occurs. In this specific region and source, for example, these areas would be larger in summer and mainly in the east, while in autumn they would be smaller and to the west and east of the source.

These results can also be used for the optimisation of a monitoring network. Usually, a major challenge is the availability of measurement instruments, which are typically placed in fixed locations (Karagulian et al., 2019). The high number of monitoring stations with a low plume detection frequency indicates that there is room to increase performance by optimising the existing monitoring network in plume detection and delineation in the early phase of a radioactivity release. In this case, there is a decrease in the number of plumes detected at stations located at distances greater than 40 km from the source. The current set of results, for example, shows seasonal variations in when the monitoring network provides the first alert and how it detects the plume as the distance from the source increases. In terms of emergency response, and in this specific case, these results would imply a redistribution of stations close to the source in autumn and a conservative approach to delineating the plume as distance from the release point increases, especially in summer. Along the same lines, this set of results could also be used to

identify areas where stations should be moved or posted to improve the spatial sampling of radiation measurements and provide a better hazard assessment in case of emergency events. For example, these results show that summer is the area statistically most affected by the passage of the plume and, therefore, some stations in the west, which are less affected during the year, could be moved to the east.

From this assessment, it appears that further improvement of the monitoring network assessment is necessary. The present analysis therefore indicated that the seasonal influence on plume dispersion causes variations in monitoring network assessment with regard to plume detection, time of first alert and maximum TGDR detection. Therefore, the assessment and optimisation of regional and national monitoring networks should take into account this influence and prior knowledge of how local/regional meteorological dynamics drive the dispersion of source emissions on a local and regional scale with time, depending on the time of year.

5. Conclusions

These results were obtained on the basis of atmospheric simulation of the same source term for a series of 1331 meteorological scenarios. For this reason, this set of results does not realistically represent the impact of a single accident at a specific nuclear power plant in a specific weather scenario. In this study, we analysed the performance of the monitoring network over a full range of recorded meteorological conditions and found that seasonal variations in meteorological conditions largely influence the area most affected by the plumes, in terms of shape and size, the time of detection (first alert) and the maximum values recorded. These differences demonstrate the need to consider the seasonal dependence of airborne radioactivity when characterising the response of the monitoring network and the need to include the influence of different meteorological conditions on the dispersion of radioactive plumes in the evaluation of monitoring networks.

Declaration of competing interest

The authors declare that they have no known competing financial interests or personal relationships that could have appeared to influence the work reported in this paper.

Data availability

The authors do not have permission to share data.

Acknowledgement

We would like to acknowledge the work or the past two decades of the EEWG, without which the EURDEP platform would not have developed as it has.

References

Abida, R., Bocquet, M., Vercauteren, N., Isnard, O., 2008. Design of a monitoring network over France in case of a radiological accidental release. Atmos. Environ. 42, 5205–5219.

Andronopoulos, S., Davakis, E., Bartzis, J., Kovalets, I., 2010. RODOS meteorological preprocessor and atmospheric dispersion model DIPCOT: a model suite for radionuclides dispersion in complex terrain. Radioprotection 45, 77–84.

Ashley, S.F., Vaughan, G.J., Nuttall, W.J., Thomas, P.J., 2017. Considerations in relation to off-site emergency procedures and response for nuclear accidents. Process Saf. Environ. Protect. 112, 77–95.

Casajus Valles, A., Marin Ferrer, M., Poljansek, K., Clark, I., 2021. *Science For Disaster Risk Management 2020* (Issue KJ-NA-30183-EN-N (Online), KJ-NA-30183-EN-C (Print)). Publications Office of the European Union.

Cinelli, A., Hernandez-Ceballos, M.A., Bossew, P., Tollefsen, T., Sanchez, I., Marín-Ferrer, M., Nishev, A., Bogučarskis, K., Gruber, V., De Cort, M., 2014. Method to estimate the terrestrial component of ambient doce equivalent rate from EURDEP routine monitoring data to improve the European Geogenic Radon Map. In: 12th International Workshop GARRM (on the Geological Aspects of radon risk mapping), 51. Book of Proceedings, 978-80-01-05548-9.

EPRI, 2012. Modular Accident Analysis Program for LWR Power Plants.

García-Marín, R., Schnabel, S., Lozano, F.J., Pulido Fernández, M., 2012. Evolución de las precipitaciones en el suroeste de la Península Ibérica (Extremadura). Nimbus: Revista de Climatología, Meteorología y Paisaje 29–30, 277–288.

Gogikar, P., Tyagi, B., 2016. Assessment of particulate matter variation during 2011–2015 over a tropical station Agra, India. Atmos. Environ. 147, 11–21.

Gogikar, P., Tyagi, B., Padhan, R.R., Mahaling, M., 2018. Particulate matter assessment using in situ observations from 2009 to 2014 over an industrial region of eastern India. Earth Syst. Environ 2, 305–322.

Guest, G., Namey, E., Chen, M., 2020. A simple method to assess and report thematic saturation in qualitative research. PLoS One 15 (5), e0232076.

Guttikunda, S.K., Gurjar, B.R., 2012. Role of meteorology in seasonality of air pollution in megacity Delhi, India. Environ. Monit. Assess. 184 (5).

Handl, G., 2020. Nuclear off-site emergency preparedness and response: key concepts and international normative principles. In: Advanced Security and Safeguarding in the Nuclear Power Industry. Elsevier, pp. 135–174.

Hernández-Ceballos, M.A., Sangiorgi, M., García-Puerta, B., Montero, M., Trueba, C., 2020. Dispersion and ground deposition of radioactive material according to airflow patterns for enhancing the preparedness to N/R emergencies. J. Environ. Radioact. 216, 106178.

Hernández-Ceballos, M.A., Sangiorgi, M., Pla, P., Jackson, K., Stucic, M., Ammirabile, L., De la Rosa Blul, J.C., De Cort, M., 2021. Impact of source term release characteristics of nuclear plant on the performance of EURDEP to identify radioactive plumes. Prog. Nucl. Energy 140, 103886.

Hoinka, K.P., De Castro, M., 2003. The Iberian Peninsula thermal low. Q. J. R. Meteorol. Soc. 129 (590) (PART A)).

IAEA, 2003. Method for Developing Arrangements for Response to a Nuclear or Radiological Emergency. INTERNATIONAL ATOMIC ENERGY AGENCY.

IAEA, 2015. IAEA Safety Standards Series No. GSR Part 7. Preparedness and Response for a Nuclear or Radiological Emergency. International Atomic Energy Agency, Vienna.

Jayamurugan, R., Kumaravel, B., Palanivelraja, S., Chockalingam, M.P., 2013. Influence of temperature, relative humidity and seasonal variability on ambient air quality in a coastal urban area. Int. J. Atmos. Sci., 264046, 2013.

Jin, X., Cai, X., Yu, M., Wang, X., Song, Y., Kang, L., Zhang, H., Zhu, T., 2021. Mesoscale structure of the atmospheric boundary layer and its impact on regional air pollution: a case study. Atmos. Environ. 258, 118511.

Karagulian, F., Gerboles, M., Barbiere, M., Kotsev, A., Lagler, F., Borowiak, A., 2019. Review of sensors for air quality monitoring. EUR 29826 EN, Publications Office of the European Union, Luxembourg, JRC116534. https://doi.org/10.2760/568261, 2019.

KIT, 2017. Karlsruhe institute of technology (KIT), 2017 JRodos Customer Guide 24. February 2017, Version 3.0.

Kopka, P., Mazur, A., Potempski, S., Wojciechowicz, H., 2022. Application of the RODOS decision support system for nuclear emergencies to the analysis of possible consequences of severe accident in distant receptors. Ann. Nucl. Energy 167, 108837.

Kovalets, I.V., Romanenko, O., Synkevych, R., 2020. Adaptation of the RODOS system for analysis of possible sources of Ru-106 detected in 2017. J. Environ. Radioact. 220–221, 106302.

Kristiansen, N.I., Stohl, A., Olivié, D.J.L., Croft, B., Søvde, O.A., Klein, H., et al., 2016. Evaluation of observed and modelled aerosol lifetimes using radioactive tracers of opportunity and an ensemble of 19 global models. Atmos. Chem. Phys. 16, 3525–3561.

Landman, C., Päsler-Sauer, J., Raskob, W., 2014. RODOS and the Fukushima Accident the Risks of Nuclear Energy Technology. Science Policy Reports. Springer Berlin Heidelberg, pp. 349–352.

Leadbetter, S.J., 2019. Use of radar rainfall to model deposition of radionuclides. Atmos. Environ. 211, 181–193.

Leung, W.H., Ma, W.M., Chan, P.K.Y., 2018. Nuclear accident consequence assessment in Hong Kong using JRODOS. J. Environ. Radioact. 183, 27–36.

Li, X., Sun, S., Hu, X., Huang, H., Li, H., Morino, Y., Wang, S., Yang, X., Shi, J., Fang, S., 2019. Source inversion of both long- and short-lived radionuclide releases from the Fukushima Daiichi nuclear accident using on-site gamma dose rates. J. Hazard Mater. 5, 120770.

Ma, Z., Ma, T., Wang, B., Li, D., Su, C., Liu, L., Hu, P., Li, Z., Chen, L., Tang, Z., 2022. Meso-scale numerical analysis for transport and deposition behaviors of radioactive aerosols under severe nuclear accident. Prog. Nucl. Energy 150, 104314.

Masson, O., Steinhauser, G., Wershofen, H., Mietelski, J.W., Fischer, H.W., Pourcelot, et al., 2018. Potential source apportionment and meteorological conditions involved in airborne 131I detections in january/february 2017 in Europe. Environ. Sci. Technol. 52, 8488–8500.

Melles, S.J., Heuvelink, G.B.M., Twenhöfel, C.J.W., van Dijk, A., Hiemstra, P.H., Baume, O., Stöhlker, U., 2011. Optimizing the spatial pattern of networks for monitoring radioactive releases. Comput. Geosci. 37, 280–288.

Mikkelsen, T., Larsen, S.E., Thykier-Nielsen, S., 1984. Description of the Risø Puff Diffusion Model. Nucl. Technol. 67, 56–65.

Mikkelsen, T., Thykier-Nielsen, S., May . Atmospheric Dis persion over Comp lex Terrain. Proceedings from the U.S. Risø National Laboratory, Roskilde, Denmark.

OECD/NEA, 2000. Monitoring and Data Management Strategies for Nuclear Emergencies. OECD Publications Service.

Ontalba, M.Á., Corbacho, J.Á., Baeza, A., Vasco, J., Caballero, J.M., Valencia, D., Baeza, J.A., 2022. Radiological Alert Network of Extremadura (RAREx) at 2021:30 years of development and current performance of real-time monitoring. Nucl. Eng. Technol. 54, 770–780.

Palau, J.L., Pérez-Landa, G., Diéguez, J.J., Monter, C., Millán, M.M., 2005. The importance of meteorological scales to forecast air pollution scenarios on coastal complex terrain. Atmos. Chem. Phys. 5, 2771–2785.

Povinec, P.P., Gera, M., Holý, K., Hirose, K., Lujaniené, G., Nakano, M., Plastino, W., Sýkora, I., Bartok, J., Gažák, M., 2013. Dispersion of Fukushima radionuclides in the global atmosphere and the ocean. Appl. Radiat. Isot. 81, 383–392.

Rudas, C., Pázmándi, T., Zagyvai, P., 2021. Evaluation of an improved method and software tool for confirming compliance with release criteria for nuclear facilities. Ann. Nucl. Energy 159, 108332.

Sangiorgi, M., Hernández-Ceballos, M.A., Jackson, K., Cinelli, G., Bogucarskis, K., De Felice, L., Patrascu, A., De Cort, M., 2020. The European radiological data exchange platform (EURDEP): 25 years of monitoring data exchange. Earth Syst. Sci. Data 12, 109–118.

Sato, Y., Sekiyama, T.T., Fang, S., Kajino, M., Quérel, A., Quélo, D., et al., 2020. A model intercomparison of atmospheric 137Cs concentrations from the Fukushima Daiichi Nuclear Power Plant accident, phase III: simulation with an identical source term and meteorological field at 1-km resolution. Atmos. Environ. X 7, 100086.

Selivanova, A., Hůlka, J., Kotík, L., Kuča, P., Rubovič, P., Malátová, I., et al., 2023. Advanced simulation techniques for the transport of routine atmospheric discharges using the JRODOS system. Prog. Nucl. Energy 157, 104596.

Song, M., Lind, M., Yang, J., Gofuku, A., 2021. Integrative decision support for accident emergency response by combining MFM and Go-Flow. Process Saf. Environ. Protect. 155, 131–144.

Thykier-Nielsen, S., Deme, S., Mikkelsen, T., 1999. Description of the Atmospheric Dispersion Module RIMPUFF. Technical Report RODOS (WG2)-TN(98)-02. Forschungszentrum Karlsruhe GMBH.

Urso, L., Astrup, P., Helle, K.B., Raskob, W., Rojas-Palma, C., Kaiser, J.C., 2012. Improving evaluation criteria for monitoring networks of weak radioactive plumes after nuclear emergencies. Environ. Model. Software 38, 108–116.

Vela-García, M., Simola, K., 2016. Evaluation of JRC source term methodology using MAAP5 as a fast-running crisis tool for a BWR4 Mark I reactor. Ann. Nucl. Energy 96, 446–454.

Yang, J.E., 2014. Fukushima dai-ichi accident: lessons learned and future actions from the risk perspectives. Nucl. Eng. Technol. 46, 27–38.

Yong, S., Linzi, Z., 2022. Robust deep auto-encoding network for real-time anomaly detection at nuclear power plants. Process Saf. Environ. Protect. 163, 438–452.

Zhuang, S., Fang, S., Goto, D., Dong, X., Xu, Y., Sheng, L., 2023. Model behavior regarding in- and below-cloud 137Cs wet scavenging following the Fukushima accident using 1-km-resolution meteorological field data. Sci. Total Environ. 872, 162165.